Journal of Materials Chemistry C

Higher conductivity in doped ethylenedioxythiophene (EDOT) dimers with chalcogen-substituted end groups

Journal:	*Journal of Materials Chemistry C*
Manuscript ID	TC-ART-06-2024-002346.R1
Article Type:	Paper
Date Submitted by the Author:	13-Jul-2024
Complete List of Authors:	Onozuka, Kota; The University of Tokyo Institute for Solid State Physics Fujino, Tomoko; The University of Tokyo, The Institute for Solid State Physics Miyamoto, Tatsuya; The University of Tokyo, Department of Advanced Materials Science Yamakawa, Takashi; The University of Tokyo Graduate School of Frontier Sciences Fundamental Science Studies Department of Advanced Materials Science Kimura Laboratory Okamoto, Hiroshi; The university of Tokyo, Applied Physics Akiba, Hiroshi; University of Tokyo Institute for Solid State Physics Yamamuro, Osamu; University of Tokyo, Institute for Solid State Physics Kayahara, Eiichi; Kyoto University, Institute for Chemical Research Yamago, Shigeru; Kyoto University, Institute for Chemical Research Oike, Hiroshi; PRESTO Mori, Hatsumi; The University of Tokyo, The Institute for Solid State Physics

SCHOLARONE™
Manuscripts

ARTICLE

Higher conductivity in doped ethylenedioxythiophene (EDOT) dimers with chalcogen-substituted end groups

Received 00th January 20xx,
Accepted 00th January 20xx

DOI: 10.1039/x0xx00000x

Kota Onozuka[a], Tomoko Fujino[a],* Tatsuya Miyamoto[b], Takashi Yamakawa[b], Hiroshi Okamoto[b], Hiroshi Akiba[a], Osamu Yamamuro[a], Eiichi Kayahara[c], Shigeru Yamago[c], Hiroshi Oike[d], and Hatsumi Mori[a]*

Conductive polymer, doped poly(3,4-ethylenedioxythiophene) (PEDOT) is a commonly employed material owing to its high conductivity, flexibility, and low-energy fabrication process. However, the broad dispersity poses challenges for understanding the conduction mechanism and designing molecules based on structure–conductivity relationships. To address this, we have focused on monodisperse oligomer conductors that provide detailed structural information owing to their crystallinity and structure control parameters involving the type, number, and sequence of monomer units, which enable the control of their electronic structures and physical properties. In this study, we investigate the effect of end groups, as another structure control parameter, on doped 3,4-ethylenedioxythiophene (EDOT) dimers, the simplest oligomers, by comparing methylthio and methylseleno groups. Substituting heavier chalcogens, from S to Se atoms, at the end groups effectively improves the electrical conductivity of doped EDOT oligomer conductors. This is due to the expansion of molecular orbitals and extension of the conjugate area of the donor, which strengthen the intermolecular interactions and bandwidth while weakening the effective Coulomb repulsion between conducting carriers. Additionally, Se-substituted end groups can induce a multiorbital system in the band structure, where the highest occupied molecular orbital (HOMO) and second HOMO (HOMO-1) bands contribute to electronic properties. Therefore, the electrical conductivities of Se-substituted oligomer salts at room temperature improve by one order of magnitude in relation to those of S-substituted oligomer salts. This approach offers guidance for designing conductors based on end groups, resulting in diverse crystal structures and electronic states that enhance conductivity.

Introduction

As next-generation materials for electronic devices, organic conductors are gaining attention owing to their lightweightness, flexibility, and solution processability in printing technologies.[1] Among these materials, conductive polymer, doped poly(3,4-ethylenedioxythiophene) (PEDOT; Fig. 1a) has been extensively employed in industries owing to its properties such as high conductivity and solution processability, making it suitable for various applications including solid electrolyte capacitors, antistatic coatings, organic electroluminescence devices, and organic solar cells.[2,3] However, achieving high conductivity typically necessitates post-treatment with solvents or strong acids.[4,5] Additionally, obtaining detailed structural information about polymer materials is challenging owing to their broad dispersity,[3] which makes it arduous to prepare single crystals. This structural inhomogeneity also makes it difficult to understand the conduction mechanism at an atomic level and design molecules based on it.

Consequently, monodisperse oligomer conductors have garnered significant interest as promising candidates for organic conductors to address these issues.[6,7] The chain length of oligomers can be precisely controlled through organic synthesis, facilitating the formation of single crystals. These crystals are instrumental in comprehending the conduction mechanism and designing molecules based on the structure–property relationship.

Furthermore, doped oligomers offer numerous structure control parameters that enable controlling electronic structures and physical properties. These parameters include the type, number, and sequence of constituent units. Additionally, end groups present promising avenues for structural control to fine-tune electronic structures and physical properties. Since the volume fraction of end groups is larger in oligomers than in polymers, the contribution of electronic effects of end groups is also larger in oligomers than in polymers.[8]

Recently, our group reported on single-crystalline 3,4-ethylenedioxythiophene (EDOT) oligomers in radical cation salts as a discrete oligomer model of doped PEDOT.[9–13] Single-crystal salts **2O•***X* (*X* = BF_4, ClO_4, and PF_6; Fig. 1b)[9] reveal one-dimensional (1D) donor stacking structures, with room-temperature resistivities (ρ_{rt}) ranging from 280–43000 ohm cm. (Fig. 1b) These elevated ρ_{rt} values result from the Mott-insulating state, where carriers are localized

[a]*The Institute for Solid State Physics, The University of Tokyo, 5-1-5 Kashiwanoha, Kashiwa, Chiba 277-8581, Japan*
[b]*Department of Advanced Materials Science, The University of Tokyo, 5-1-5 Kashiwanoha, Kashiwa, Chiba 277-8561, Japan*
[c]*Institute for Chemical Research, Kyoto University, Uji, Kyoto 611-0011, Japan*
[d]*PRESTO, Japan Science and Technology Agency (JST), Kawaguchi, Saitama 332-0012, Japan*

Electronic Supplementary Information (ESI) available: theoretical calculations, single-crystal X-ray diffraction analyses, magnetic measurements, differential scattering calorimetry, and NMR measurements. See DOI: 10.1039/x0xx00000x

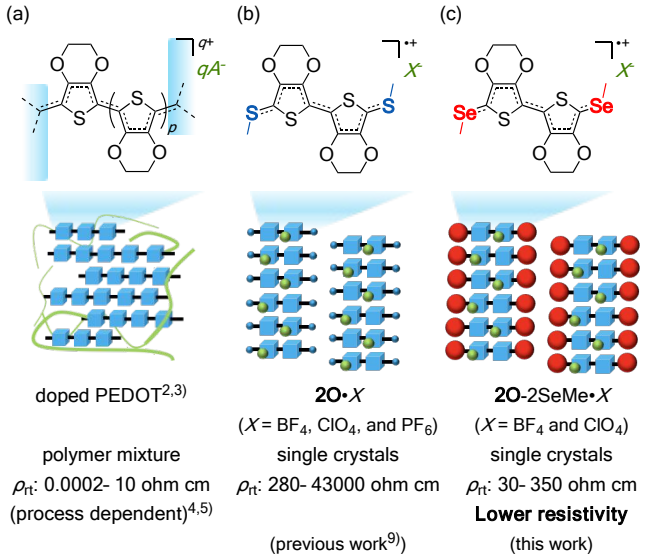

Fig. 1. Chemical structures and illustration of the packing structures of (a) doped PEDOT, (b) **2O**•*X*,[9] and (c) **2O**-2SeMe•*X*. Green lines and spheres represent anions. Blue and red spheres represent the methylthio and methylseleno groups of the oligomers, respectively.

owing to the effective Coulomb repulsion between conducting carriers ($\boldsymbol{U}_{\mathbf{eff}}$).[14,15] To deviate from the Mott-insulating state and improve conductivity, the Mott gap should be decreased by increasing intermolecular orbital overlapping (***W*** : bandwidth) or decreasing $\boldsymbol{U}_{\mathbf{eff}}$.[16] We previously reported the reduction of $\boldsymbol{U}_{\mathbf{eff}}$ by expanding the conjugate system achieved by extending the oligomer chain length, which led to increased conductivity. For instance, elongating from a dimer (**2O**) to trimer (**3O**) resulted in a tenfold increase in the conductivity of **3O**•$PF_6(CH_2Cl_2)_n$ in relation to that of **2O**•PF_6, despite the weakly dimerized structure of **3O**•$PF_6(CH_2Cl_2)_n$.[10] More recently, we elongated the chain length to a tetramer (**4PS**) using a mixed sequence and further modulated the band-filling in a **4PS**$(PF_6)_{1.2}(solvent)_m$ by controlling the stacking structure. These combined effects led to a six-order of magnitude improvement in room-temperature conductivity in relation to that of **2O**•PF_6 and the realization of a metallic state above room temperature.[12] Although a decrease in $\boldsymbol{U}_{\mathbf{eff}}$ was achieved by increasing the chain length and band-filling modulation, the ***W*** of **4PS**$(PF_6)_{1.2}(solvent)_m$ decreased to 0.41 eV because of the increased stacking distance and one unit slipping stacking for **4PS**$(PF_6)_{1.2}(solvent)_m$. Furthermore, enhancing conductivity at room temperature necessitates an increase in ***W*** and a decrease in $\boldsymbol{U}_{\mathbf{eff}}$, thereby necessitating a decrease in $\boldsymbol{U}_{\mathbf{eff}}/\boldsymbol{W}$.

In this study, we focused on examining the effect of little-explored end groups on the reduction in $\boldsymbol{U}_{\mathbf{eff}}/\boldsymbol{W}$ among oligomer-based conductors. Although previous studies have delved on synthesizing various end groups in EDOT oligomers, such as phenyl and alkyl groups,[7,17,18] their focus has been on synthetic methods or radical cation behavior in solutions. The impact of end groups on physical properties in solids, particularly in single crystals, has been largely overlooked,[7] thereby impeding efforts to control physical properties via electron correlation parameters ($\boldsymbol{U}_{\mathbf{eff}}/\boldsymbol{W}$). In our investigation, we explored the effect of end groups on a doped EDOT dimer by replacing methylthio (SMe) groups with methylseleno (SeMe) groups (i.e., replacing S atoms with Se atoms: **2O**-2SeMe•*X*, where *X* = BF_4 and ClO_4, as shown in Fig. 1c). Notably, this chalcogen substitution led to the expansion of molecular orbital and conjugate area in the doped oligomers, consequently increasing the intermolecular interactions and ***W***, while reducing $\boldsymbol{U}_{\mathbf{eff}}$ and $\boldsymbol{U}_{\mathbf{eff}}/\boldsymbol{W}$. As a result, the conductivity of the salts increased significantly, similar to the increase in conductivity observed when the chain length is extended from a dimer (**2O**•*X*) to trimer (**3O**•*X*).[10] This study underscores the potential of tuning the physical properties of oligomer conductors by manipulating the end groups. This approach will promote the formation of diverse crystal structures and electronic states that can improve conductivity, thus offering valuable insights into the design of conductors based on end groups.

Results and discussion

Molecular design

First, we examined the contribution of the end groups of donors to the electronic structures for the SMe-substituted **2O**•*X* single crystals. Previous studies utilizing density functional theory (DFT) calculations have shown that the highest occupied crystal orbital (HOCO) is distributed on the S atoms in the SMe group.[9] This crystal orbital corresponds to that of singly occupied molecular orbitals (SOMO) of the isolated donor **2O** in the radical cation state (Fig. 2a and 2c),[9] calculated by the Gaussian 16 software[19] at the (U)B3LYP/6-31G(d) level, potentially stabilizing the molecule in the oxidized state. Therefore, we investigated the effect of substituting chalcogen atoms from S atom of the SMe end groups with heavier Se or Te atoms on conducting properties. DFT calculations of SOMO for SeMe- and TeMe-substituted EDOT dimer (i.e., **2O**-2SeMe and **2O**-2TeMe) in radical cation forms revealed complete delocalization of the molecular orbitals across the molecules, including on the Se and Te atoms in the end groups (Fig. 2b and 2d, Fig. S1 and S2, Table S3 and S4, ESI†). The SOMO expanded in the order **2O**, **2O**-2SeMe, and **2O**-2TeMe owing to the larger atomic radius from S, Se, to Te atoms. This trend was also observed for another skeleton, 3,4-ethylenedithiothiophene dimer **2S**[20] with chalcogen-substituted end groups (Fig. S1 and S2, Table S5 and S6, ESI†). The expanded conjugated area provided by the heavier chalcogen substitution is expected to further decrease $\boldsymbol{U}_{\mathbf{eff}}$ and increase ***W***, thereby decreasing $\boldsymbol{U}_{\mathbf{eff}}/\boldsymbol{W}$ to improve conductivity.

Synthetic procedures

The synthesis began with an unsubstituted EDOT dimer **2O**-2H (Scheme 1). This compound was lithiated with *n*-butyllithium and then reacted with dimethyl diselenide, yielding **2O**-2SeMe in 80% yield for the two-step transformations (Scheme 1a, Fig. S18 and S19, ESI†). The structural integrity of the neutral **2O**-2SeMe was confirmed by X-ray diffraction (XRD) analyses of single crystals prepared via liquid-liquid diffusion from ethanol and dichloromethane (Fig. S3, Table S1, ESI†). Single crystals of the doped dimer **2O**-2SeMe•*X* (*X* = BF_4, ClO_4) were further prepared by electrocrystallization of **2O**-2SeMe in tetrahydrofuran (THF) in the

 This journal is © The Royal Society of Chemistry 20xx

Please do not adjust margins

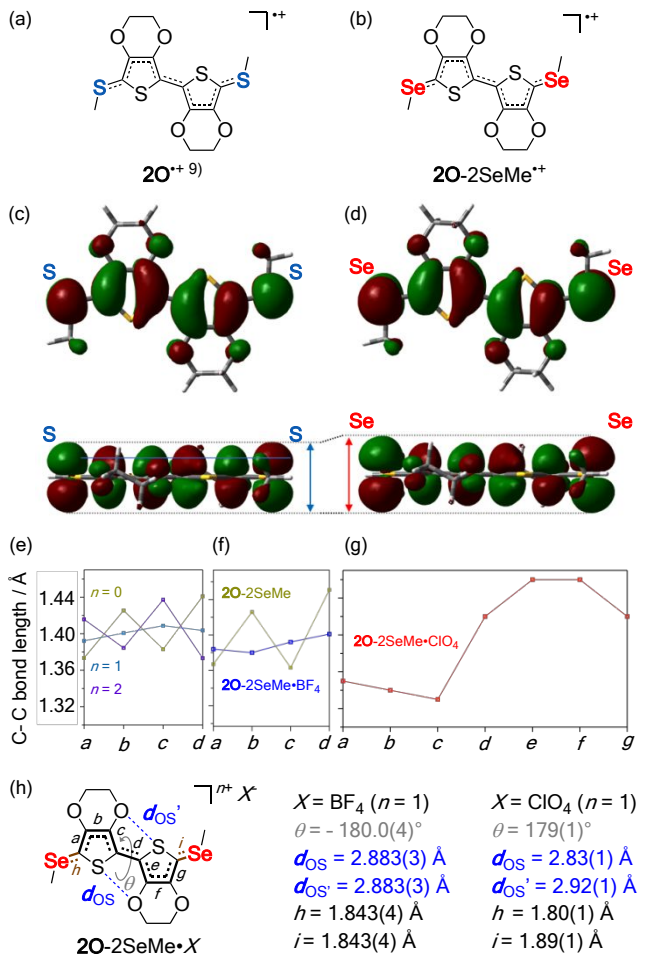

Fig. 2. Molecular structures and calculated SOMOs of DFT-optimized radical cations of (a)(c) **2O**•+ [9] and (b)(d) **2O**-2SeMe•+. Calculations were performed using Gaussian 16[19] at the (U)B3LYP/6-31G(d) level. Details are provided in ESI†. (e) DFT-calculated C–C bond lengths of the salts depending on the charge-transfer degree *n*. The C–C bond lengths observed in the single-crystal structures of (f) **2O**-2SeMe, **2O**-2SeMe•BF_4, and (g) **2O**-2SeMe•ClO_4 at 293 K. (h) Structural details of donors in the single crystals of **2O**-2SeMe•BF_4 and **2O**-2SeMe•ClO_4.

presence of tetra-*n*-butylammonium tetrafluoroborate or perchlorate as the electrolyte at a constant current of 0.25 μA. The shape of the single crystals was needle-like, and their color was dark green. The synthesis of **2O**-TeMe followed a synthetic route similar to that used for **2O**-SeMe. However, an insoluble white solid in typical organic solvents was obtained, hindering the subsequent electrolytic oxidation process. To enhance solubility, we substituted a highly soluble donor **2S**,[20] for **2O**, which has a twisted structure in the neutral state, providing the donor with high solubility and stability. Thus, **2S**-2Br was lithiated and then TeMe groups were introduced by reaction with dimethyl ditelluride, resulting in **2S**-2TeMe in 83% yield for the two-step transformations (Scheme 1b, Fig. S20 and S21, ESI†). We then attempted to electrochemically oxidize the donor in the presence of various electrolytes such as tetra-*n*-butylammonium salts in various organic solvents. However, single crystals of radical cationic salts were not obtained, possibly owing to the instability of the dimer during the electrochemical reaction.

Single-crystal structure of 2O-2SeMe•*X*

Single-crystal X-ray structure analyses of **2O**-2SeMe salts at 293 K revealed a 1:1 composition of the oxidized **2O**-2SeMe and the counter anion BF_4^- or ClO_4^- (Fig. 3a, Fig. S4 and S5, Table 1, Table S1, ESI†),[21] confirming the charge-transfer degree of **2O**-2SeMe donor to be +1 in the salts (i.e., monovalent radical cation **2O**-2SeMe•+). As for **2O**-2SeMe•BF_4, the crystal space group is *I*2/*a*, which is isostructural to **2O**•BF_4.[9] A half of the donor molecule and a half of the anion were crystallographically independent. The inversion center and the glide plane were at the center of the donor molecule and 1D donor stacking was observed. In contrast, **2O**-2SeMe•ClO_4 has a space group of *I*a, which differs from those of **2O**-2SeMe•BF_4 and **2O**•*X* (*X* = BF_4, ClO_4).[9] A single donor molecule and an anion were crystallographically independent without an inversion center at the donor molecules, and a 1D donor stacking structure was observed (Table S1, Fig. S4 and S5, ESI†).

The atomic-level structures of donor molecules were further analyzed through bond-length analyses. A comparison of the bond lengths of the single-crystal structures with those of the DFT-predicted structures revealed a dependence on the charge-transfer degree (*n* in Fig. 2h). The DFT-optimized structures of **2O**-2SeMe simulated the bond lengths in the neutral state (*n* = 0), radical cation state (*n* = 1), and dication state (*n* = 2) at the (U)B3LYP/6-31G(d) level using the Gaussian 16 software.[19] For *n* = 0, C–C bond lengths *a* and *c* are significantly shorter compared to *b* and *d*, indicating the double-bond character (Fig. 2e, Table S7, ESI†), for which the contribution of the benzenoid structure is dominant. For *n* = 1, bond lengths *a*–*d* are comparable owing to the resonance structure (Table S3, ESI†). For *n* = 2, bond lengths *a* and *c* are significantly longer compared to *b* and *d*, indicating the single-bond character on the basis of the quinoid structure (Table S8, ESI†). With reference to these predictions, the degree of the bond-length alterations observed in single-crystal **2O**-2SeMe and **2O**-2SeMe•BF_4 was comparable to that simulated for *n* = 0 and 1, respectively (Fig. 2f). In contrast, the bond-length alteration

Scheme 1. Syntheses of neutral dimers, (a) **2O**-2SeMe and (b) **2S**-2TeMe, and their charge-transfer salts. [a]Conditions for anodic oxidation. (+) Pt | Pt (–), ^{n}Bu$_4$N•*X*, THF, 30 °C, 0.25 μA.

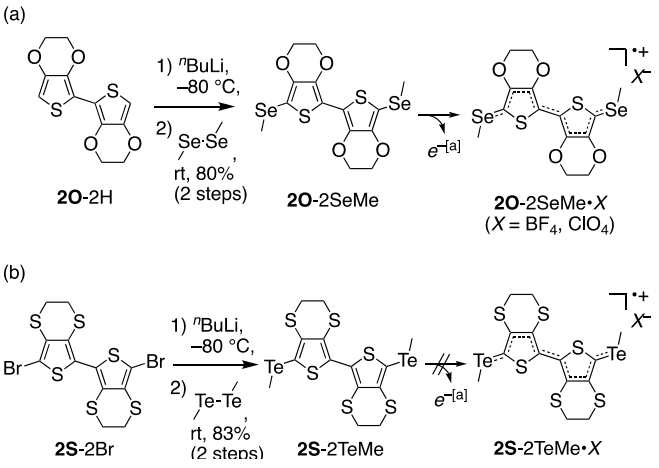

Please do not adjust margins

Table 1. Physical properties and structural data for single crystals of **2O**•BF_4, **2O**•ClO_4, **2O**-2SeMe•BF_4, and **2O**-2SeMe•ClO_4.

Compound	**2O**•BF_4[9]	**2O**•ClO_4[9]	**2O**-2SeMe•BF_4	**2O**-2SeMe•ClO_4
Space group, *Z*	*I*2/*a*, 4	*I*2/*a*, 4	*I*2/*a*, 4	*Ia*, 4
Donor valency	1	1	1	1
Interplanar distance between donors[a] (Å)	3.462	3.471	3.494	3.507
ρ at room temperature (experimental) (ohm cm)[b]	280	4300	30	350
E_a (experimental) (eV)	0.177	0.224	0.100	0.235
W (calculated by OpenMX[24]) (eV)	0.998	0.959	1.15	1.13
U_{eff}^{exp} [c] (eV) from E_a (experimental) and ***W*** (calculated)	1.35	1.41	1.35	1.60[e]
U_{eff}^{exp} [c]/***W***	1.35	1.47	1.17	1.41[e]
Intracolumnar transfer integral ***t*** (meV)	239	250	285	268
Peak-top energy of reflectivity (experimental) (eV)[d]	0.74	0.74	0.67	0.64

[a]Interplanar distances were measured between the geometric center of the bithiophene ten atoms in **2O** or **2O**-2SeMe and the mean plane composed of the bithiophene ten atoms in the facing donor. [b]Minimal value among three samples. [c]$U_{eff}^{exp} = W + 2E_a$. [d]Electric field was applied along each π-stacking direction. [e]Since **2O**-2SeMe•ClO_4 is not isostructural to **2O**•BF_4, **2O**•ClO_4, and **2O**-2SeMe•BF_4, the U_{eff}^{exp} value cannot be directly compared with those of other salts.

for single-crystal **2O**-2SeMe•ClO_4 was different from that simulated for n = 1, although the n value was determined to be 1 by the ratio of donor and anion in the single crystals structure (Table 1, Table S1, Fig. S5, ESI†). Observed lengths *a*–*c* are shorter compared to *d*–*g*, indicating stronger double-bond character (1.32–1.36 Å) similar to that in the case of n = 0, while *d*–*g* were longer (1.41–1.45 Å) similar to that in the case of n = 2 (Fig. 2g), indicating the asymmetric molecular structure. This observation implies intramolecular charge localization, as has been suggested for the elongated oligomer (tetramer) salt with SMe end groups at low temperatures.[12] The charge localization in the donor molecule, which has never been observed in short oligomers such as dimer and trimer salts, can be characteristic of heavier atom-substituted oligomers that may contribute toward expanding the conjugate area (Fig. 2c and 2d).

The π-stacking distance between donor molecules in **2O**-2SeMe•BF_4 is 3.494 Å (Fig. 3b), which is larger than that in **2O**•BF_4 (3.462 Å).[9] Moreover, in **2O**-2SeMe•ClO_4, the π-stacking distance is 3.507 Å, which is larger than that in **2O**•ClO_4 (3.471 Å)[9] because of the substitution with larger Se atoms in relation to that with S atoms. The distances between Se–Se atoms in the donor stacking direction are 3.5604(6) and 3.6315(6) Å for **2O**-2SeMe•BF_4 and 3.568(1) Å and 3.647(1) Å for **2O**-2SeMe•ClO_4 (Fig. 3b, Fig. S6, ESI†). These values are larger than the S–S distances observed for **2O**•*X* (**2O**•BF_4: 3.521(1) and 3.572(1) Å and **2O**•ClO_4: 3.5227(8) and 3.5878(9) Å).[9] These distances are shorter than double the van der Waals radius, d_{SeSe} = 3.80 Å and d_{SS} = 3.60 Å, respectively.[22] The percentage of d_{SS} to double the van der Waals radius of **2O**•BF_4 is 99% and that of d_{SeSe} for **2O**-2SeMe•BF_4 is 95%; the lower percentage for **2O**-2SeMe•BF_4 implies increased intermolecular interactions between donors.

First-principles calculations

The increase in intermolecular interactions of **2O**-SeMe•BF_4 and **2O**-SeMe•ClO_4 in relation to that of their counterparts was theoretically confirmed. We calculated intracolumnar transfer integrals for the two nearest intracolumnar donors (***t*** in Fig. 3b; Fig. S9, Table S2, ESI†) using the Amsterdam Density Functional (ADF) software,[23] which were found to be 285 and 268 meV, respectively. These values are

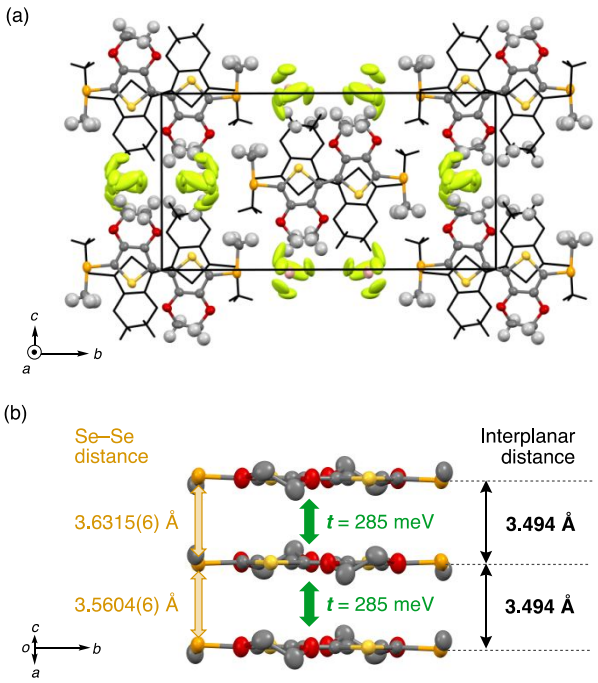

Fig. 3. Single-crystal structures **2O**-2SeMe•BF_4 at 293 K along (a) the *a*-axis and (b) the direction perpendicular to the molecular π-plane drawn by Mercury[21] (see ESI† for the details). Yellow: S, yellowish green: F, red: O, grey: C, pink: B, orange: Se, light gray: H. ORTEP drawings (50% thermal ellipsoid) were shown for the upright molecules with black wires for the upside-down molecules in (a). The interplanar distances were measured between the centroid of the ten atoms in the bithiophene of a donor and the mean planes composed of ten atoms in the bithiophene of the facing donor. Green arrows represent transfer integrals (***t***) for the intracolumnar interactions between the two nearest molecules. H atoms are omitted for clarity in (b).

This journal is © The Royal Society of Chemistry 20xx

Please do not adjust margins

larger than that of **2O**•BF_4 (238 meV) and **2O**•ClO_4 (250 meV; Fig. S9, Table S2, ESI†). On the other hand, the intercolumnar transfer integral was less than 1 meV, indicating that **2O**-SeMe•*X* has 1D intermolecular interaction (Fig. S9, Table S2, ESI†).

The band structures of **2O**-2SeMe•*X* were calculated using the first-principles calculation OpenMX software package,[24] where electron correlations near the Fermi level are not considered. The calculation results revealed a metallic 1D band dispersion, the density of states (DOS), and the Fermi surface without a gap at the Fermi level (Fig. S12 and S13 ESI†). The ***W*** value, based on the DOS of **2O**-2SeMe•BF_4 was 1.153 eV (Fig. 4, Fig. S12a, ESI†). This value exceeds that of **2O**•BF_4 (0.998 eV),[9] as predicted by the increased ***t*** values. The ***W*** value based on the DOS of **2O**-2SeMe•ClO_4 was 1.133 eV (Fig. S10 and S12b, ESI†), exceeding that of **2O**•ClO_4 (0.959 eV).[9] These results suggest that chalcogen substitution causes an increase in ***t*** and the corresponding ***W*** possibly owing to the enhanced intermolecular orbital interactions through the Se–Se interactions although the π-stacking distance increased.

Notably, an inversion between the HOMO-derived and HOMO−1-derived bands was observed near −0.4 eV around the Γ point in **2O**-SeMe•*X* (Fig. 4, Fig. S10, ESI†). This band inversion might result from the expansion of the conjugate area, which highly disperses the HOMO-derived band. The crossing HOMO and HOMO−1 bands may form a multiorbital system,[25–28] potentially contributing to the electronic structures in contrast to the S-substituted analogs.

Additionally, the crystal orbitals of **2O**-2SeMe•BF_4 derived from the HOCO band at the Γ point corresponded to the SOMO of the **2O**-2SeMe radical cation (Fig. 2d, Table S3, ESI†) and extended to the Se atoms of both end groups. The orbital distribution was also observed for **2O**-2SeMe•ClO_4 (Fig. S11, ESI†) in which the charge was localized in an intramolecular manner, as apparent in the bond-length analyses (Fig. 2g). The extended crystal orbitals to the entire donor molecule observed for both **2O**-2SeMe•BF_4 and **2O**-2SeMe•ClO_4 may expand the conjugate area of donor in relation to those for SMe-substituted **2O**•BF_4 and **2O**•ClO_4.

Optical characteristics

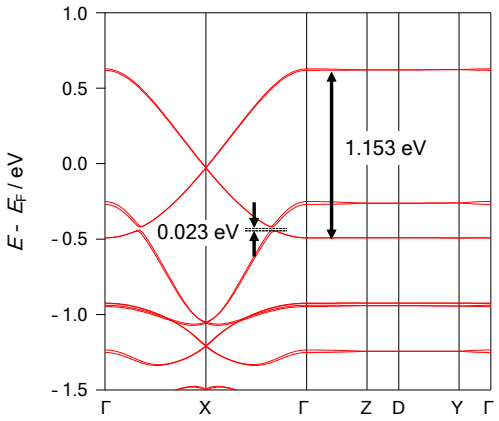

Fig. 4. Band structure of **2O**-2SeMe•BF_4 calculated by using OpenMX[24] based on the single-crystal structure excluding the disordered BF_4 anion. Γ (0,0,0), X (0.5,0,0), Z (0,0.5, –0.5), D (0.0,0.5,0.5). See Experimental section for the calculation details.

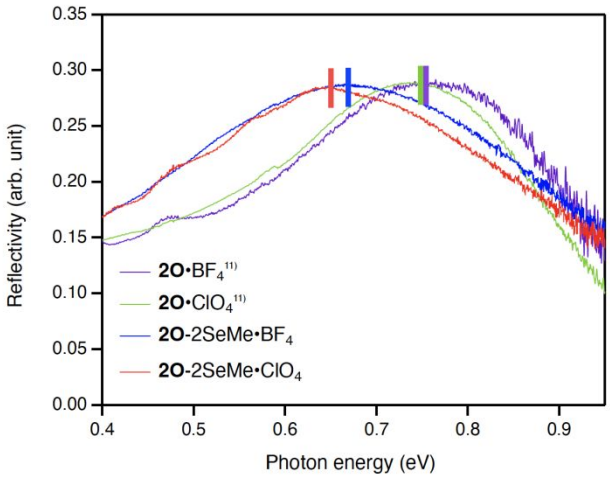

Fig. 5. Polarized reflectivity spectra of **2O**•BF_4,[11] **2O**•ClO_4,[11] **2O**-2SeMe•BF_4, and **2O**-2SeMe•ClO_4 single crystals. The electric field was applied along each π-stacking direction. The bars indicate the peak top energies.

Considering the extended crystal orbitals encompassing the entire donor molecule, including end groups, substituting chalcogen atoms with heavier, large-sized Se atoms in the π-conjugate system may lead to a decrease in the effective on-site Coulomb interaction (U_{eff}). To explore these effects, we investigated the Se-substitution effects on U_{eff} by analyzing polarized infrared (IR) reflectivity spectra of the radical cation salts. We measured the reflectivity of single-crystal **2O**-SeMe•BF_4 and **2O**-SeMe•ClO_4 at room temperature with respect to the π-stacking direction. The peak top energies associated with the optical Mott gap were determined to be 0.67 eV for **2O**-SeMe•BF_4 and 0.64 eV for **2O**-SeMe•ClO_4 (Fig. 5, Table 1). These values for **2O**-SeMe•*X* were lower than those for **2O**•*X* (**2O**•BF_4: 0.74 eV and **2O**•ClO_4: 0.74 eV).[11] These results suggest that the optical Mott gap efficiently decreases, indicating a decrease in the corresponding U_{eff}. The combined effects of an increase in ***W*** and a decrease in U_{eff} lead to a favorable reduction in U_{eff}/W, thereby enhancing the conductive properties.

Magnetic properties

Further insights into the electronic structures were gained through magnetic property measurement. The static magnetic susceptibility (χ) of **2O**-2SeMe•*X* (*X* = BF_4 and ClO_4) polycrystals was measured using a superconducting quantum interference device (SQUID) in the temperature range of 4.2–300 K. For **2O**-SeMe•BF_4, χ at 300 K was found to be 9.69×10^{-5} emu mol^{-1}. These values gradually decreased with decreasing temperature, experiencing a drop of approximately 20% at around 170 K, followed by a rapid increase below 50 K (Fig. S14a, ESI†). For **2O**-2SeMe•ClO_4, the χ at 300 K was 1.77×10^{-4} emu mol^{-1}, which decreased slowly with lowering temperature, reducing by approximately 20% at around 170 K, and then increasing rapidly below 50 K (Fig. S14b, ESI†). To understand the origin of the decrease in χ at around 170 K, single-crystal X-ray structure analysis was conducted below transition temperatures at 123 K for **2O**-2SeMe•BF_4 and 133 K for **2O**-2SeMe•ClO_4 (Table S1, Fig. S7 and S8, ESI†) The analysis of both salts revealed molecular dimerization

Please do not adjust margins

where the glide planes disappeared. This stacking dimerization can be attributed to the instability of the 1D electronic structure, as observed for **2O**•*X*.[9] The remaining χ (approximately 80%) after the transition around 170 K can be attributed to the formation of the multiorbital system[25–28] originating from the inversion of HOMO and HOMO−1 bands (Fig. 4, Fig. S10, ESI†). The increase observed below 50 K may be due to Curie impurities.

Electrical resistivity

The decrease in U_{eff}/W due to the heavier chalcogen substitution, as suggested by DFT calculations based on single-crystal structures and optical measurement, effectively reduced electrical resistivity (ρ). The ρ values were measured for **2O**-2SeMe•*X* using the two-probe method. The ρ_{rt} value of **2O**-SeMe•BF_4 was 30 ohm cm (Fig. 6), which is an order of magnitude lower than that of **2O**•BF_4, which was 280 ohm cm.[9] This compound exhibited semiconducting behavior with an activation energy (E_a) of 0.100 eV in the temperature range of 184–300 K (Table 1), a value lower than that of **2O**•BF_4 (0.177 eV).[9] Moreover, a significant increase in ρ was observed at approximately 170 K, attributed to stacking dimerization, as indicated by single-crystal X-ray structural analysis at 117 K and a rapid drop in χ around 170 K. Differential scanning calorimetry (DSC; Fig. S16 and S17, ESI†) also revealed an exothermic peak, suggesting a phase transition in this temperature range for polycrystals. Nearly no hysteresis of resistivity was observed during the cooling and heating processes, suggesting a nearly second-order phase transition accompanying the structural change.

On the other hand, the ρ_{rt} of **2O**-2SeMe•ClO_4 was 350 ohm cm, an order of magnitude lower than that of **2O**•ClO_4, which was 4300 ohm cm (Fig. 6, Table 1).[9] Semiconducting behavior was also observed for **2O**-2SeMe•ClO_4 with E_a = 0.235 eV, exceeding that of **2O**•ClO_4 (0.223 eV).[9] Although the crystal structure analysis of SMe-substituted donor **2O** in **2O**•ClO_4 was symmetric with a glide plane at the center

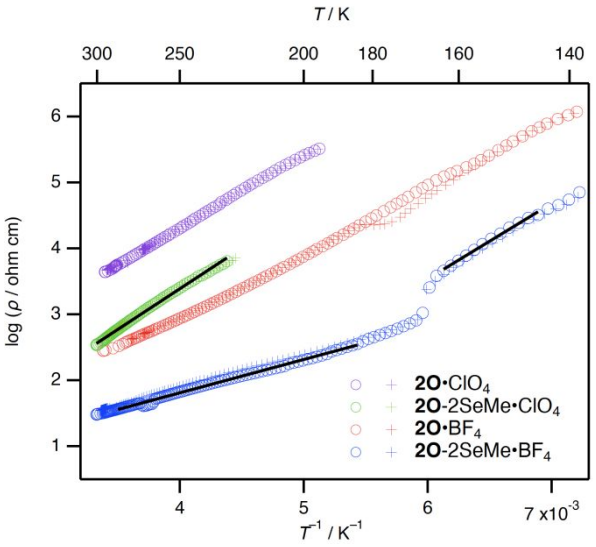

Fig. 6. ρ–T^{-1} plot for **2O**•BF_4, **2O**•ClO_4, **2O**-2SeMe•BF_4, and **2O**-2SeMe•ClO_4. The data for heating and cooling processes are shown in crosses and circles, respectively. The solid black lines are fitting to the data with an Arrhenius plot.

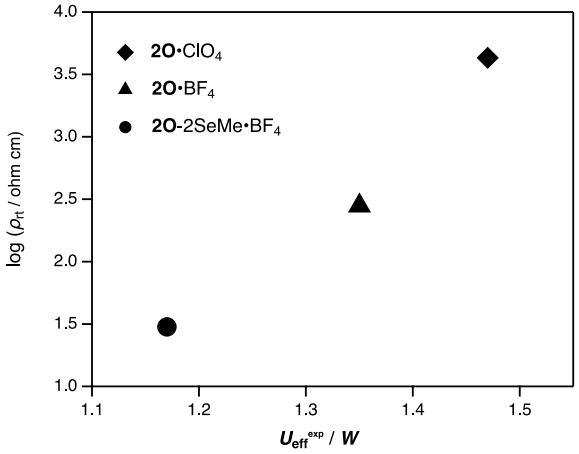

Fig. 7. Electrical resistivity of isostructural **2O**•ClO_4, **2O**•BF_4 and **2O**-2SeMe•BF_4 at room temperature as a function of U_{eff}^{exp}/W.

of the molecule at 293 K,[9] the Se-substituted donor **2O**-2SeMe in **2O**-2SeMe•ClO_4 was asymmetric with charge localization in the molecule. This intramolecular charge localization might account for the slightly increased E_a of **2O**-2SeMe•ClO_4 in relation to that of **2O**•ClO_4.

Comparative discussion of 2O-2SeMe•X with 2O•*X*

Finally, we discuss the impact of chalcogen substitution in the end groups on syntheses, crystal and electronic structures, and the physical properties. Despite the increased stacking distances from **2O**•*X* to Se-substituted **2O**-2SeMe•*X* (*X* = BF_4, ClO_4), the introduction of heavier chalcogen atoms led to enhanced intermolecular interactions. DFT calculations also revealed an increased transfer integral and ***W***. Notably, an inversion of the HOMO and HOMO−1 bands around the Γ point was observed in **2O**-2SeMe•*X* owing to the expansion of the conjugate area, resulting in a characteristic multiorbital system in the band structure.[25–28] Moreover, polarized reflectivity spectra, when applying the electric field along each π-stacking direction, indicated a reduction in the optical Mott gap energy in **2O**-2SeMe•*X* in relation to that in **2O**•*X*, leading to a decrease in U_{eff}. This dual effect of increasing ***W*** and decreasing U_{eff} effectively reduced U_{eff}/W. As a result, the ρ_{rt} values of **2O**-2SeMe•*X* decreased by one order of magnitude in relation to that of **2O**•*X*. This one-order decrease is almost similar to the decrease observed from the dimer salt (**2O**•PF_6) to the trimer salt (**3O**•$PF_6(CH_2Cl_2)_n$), extending the conjugate chain length.[10] For the three isostructural salts with *I*2/*a* (i.e., **2O**•ClO_4, **2O**•BF_4, and **2O**-2SeMe•BF_4), the electron correlation parameter, U_{eff}^{exp}/W [= (W + 2E_a)/W,[14] as suggested by ***W*** derived from the first-principles calculations and E_a from resistivity measurement, decreased in the order **2O**•ClO_4 (1.47), **2O**•BF_4 (1.35), and **2O**-2SeMe•BF_4 (1.17) (Table 1). As evident from Fig. 7, the electrical resistivity at room temperature decreased with the lowering of the electronic correlation parameter, U_{eff}^{exp}/W, from **2O**•ClO_4, **2O**•BF_4, to **2O**-2SeMe•BF_4, owing to the heavier chalcogen substitution of the end groups and anion effects. These

 This journal is © The Royal Society of Chemistry 20xx

Please do not adjust margins

results indicate that increasing the conjugated area due to heavier chalcogen substitution effectively reduces U_{eff}/W and increases conductivity.

Experimental section

Apparatus

Single-crystal XRD was performed using a Rigaku HyPix-6000HE X-ray diffractometer (Mo K_α, λ = 0.71073 Å). Resistivity measurement was performed using a HUSO HECS 994C instrument with a direct current/voltage generator (ADVANTEST R6142), and digital multimeter (KEYTHELY 2001). Microscopic mid-IR and ultraviolet-visible (UV–vis) spectroscopy was performed using an IRT-5000 (JASCO) equipped with FT/IR-6100 (JASCO) and MSV-5200TSO (JASCO), respectively. Static magnetic susceptibility measurement was conducted using a Quantum Design SQUID magnetometer (MPMS-XL). DSC was performed using a Diamond DSC (PerkinElmer, Inc.).

Materials

The reagents were purchased from commercial suppliers and used as received. **2O**-2SeMe and **2S**-2TeMe was synthesized in an argon atmosphere (see ESI† for the details). The single crystals of **2O**-2SeMe•*X* were prepared using an electrocrystallization method.

Single-crystal XRD structural analyses

The single-crystal structures were obtained using a direct method (SHELXT[29] version 2018/2) and refined using the full-matrix least-squares technique (SHELXL version 2018/3) using the Olex2-1.2 (OlexSys) software.[30] Anisotropic thermal parameters were applied to all non-hydrogen atoms. Hydrogen atoms were geometrically generated.

Theoretical calculations

Electronic structures of isolated molecules

All calculations were performed on the Gaussian 16 program[19] at the DFT level with the unrestricted B3LYP functional, the gradient correction of the exchange functional by Becke,[31,32] and the correlation functional by Lee et al.[33] The 6-31G(d) split valence plus a polarization basis set was used for H, C, O, S, and Se.[34,35] SDD basis[36] set was used for Te. The cartesian coordinates for the optimized geometries are presented in Table S3–S8, ESI†. The calculated results of **2O**-2SeMe, **2O**-2TeMe, and 2**S**-2TeMe radical cations are shown in Fig. 2c and 2d, Fig. S1, ESI†. Orbital shapes were visualized using GaussView 6.0.[37]

Electronic structures of single crystals

All periodic DFT calculations were performed using the OpenMX[24] software based on optimized localized basis functions and pseudopotentials (PPs). The basic functions used were H6.0-s2p1, C6.0-s2p2d1, O6.0-s2p2d1, S7.0-s2p2d1f1, and Se7.0-s3p2d1 for hydrogen, carbon, oxygen, sulfur, and selenium, respectively. The radial functions were optimized using a variational optimization method.[38,39] For valence electrons in PPs, we included 1s for hydrogen, 2s and 2p for carbon and oxygen, and 3s and 3p for sulfur, respectively. All the PPs and pseudoatomic orbitals used in the study were taken from the database (2019) on the OpenMX website,[24] which was benchmarked using the delta gauge method.[40] Real-space grid techniques were used for the numerical integrations and solution of the Poisson equation using an FFT with an energy cutoff of 220 Ryd. Brillouin zone integrations were performed on a 6 × 2 × 2 or 3 × 1 × 1 *k*-grid, and the Fermi–Dirac distribution function at 300 K was employed as a smeared occupation function. We used the generalized gradient approximations proposed by Perdew, Burke, and Ernzerhof as the exchange-correlation functional.[41] In the calculations, we utilized the geometry of the single-crystal structure of **2O**-2SeMe•*X* at 293 K, excluding the anion structures, without prior structural optimization. The system charge was set to +2.0 (+1 per donor molecule) for those instances where anionic structures were excluded, in order to maintain charge balance. Crystal orbitals at the Γ point (0, 0, 0) were drawn by VESTA[42] (Fig. S11, ESI†).

Transfer integrals in the single-crystal structures

Transfer integrals between neighboring molecules (Fig. S9, ESI†) were calculated using ADF program[23] at the GGA:PW91[43]/TZP[44] level using the HOMO generated from the experimental crystal geometries of **2O**•*X* and **2O**-2SeMe•*X*. The intermolecular values for these salts are shown in Table 1 and Table S2.

Electrical resistivity measurement

Temperature-dependent ρ measurement of the **2O**-2SeMe•*X* single crystal was performed using a two-probe method. The sample was prepared by connecting gold wires (15 mm in diameter) to both ends of the single crystal along its long axis (the *a*-axis) using conductive carbon paste. To achieve suitable hardness, each conductive paste was mixed with ethylene glycol monobutyl ether acetate prior to use. Additionally, each gold wire was connected to another gold wire using silver paste as a buffer to minimize mechanical stress on the sample during measurement, and both ends of the wires were bridged to the electrode using silver paste. Prior to the temperature-dependent resistance (ρ) measurement, the ohmic behavior of the samples was confirmed by examining the current–voltage characteristics at room temperature from −1 to 1 V. At a constant DC voltage of 0.5 V within the ohmic region (Fig. S15, ESI†), the temperature-dependent resistance *R* of the sample was measured after cooling from room temperature to approximately 10 K, followed by heating to room temperature at a rate of approximately 1 K min^{-1} to obtain the ρ–*T* plot. The plot was then fitted using the Arrhenius model, expressed as $\log \rho = a + b^*(1/T)$, to estimate the activation energy (E_a in Table 1).

DSC

DSC for polycrystals of **2O**-2SeMe•*X* (*X* = BF_4, ClO_4) were performed under a nitrogen atmosphere. The measurement was performed within a temperature range of 100 to 298 K, utilizing a cooling and heating rate of 5 K min^{-1} (Fig. S16 and S17, ESI†).

Optical reflection spectroscopy

The steady-state polarized reflectivity spectra in the mid-IR region (0.08–0.97 eV) and UV–vis–near IR region (0.46–6.2 eV) were analyzed using mid-IR and UV–vis spectrometers equipped with a polarizer. The spectra were obtained by applying an electric field (*E*) perpendicular to the π-stacking direction, which is the *a*-axis for **2O**-2SeMe•X compounds (where *X* = BF_4 and ClO_4).

Static magnetic susceptibility measurement

The static magnetic susceptibility of the polycrystalline samples of **2O**-2SeMe•*X* was measured by subjecting the samples to a static magnetic field of 50,000 O_e upon cooling the sample from 300 to 50 K at a rate of 2 K min^{-1}, from 49 to 10 K at 1 K min^{-1}, and from 10 to 2 K at 0.5 K min^{-1} (Fig. S14, ESI†).

Conclusion

In this study, we established a method for chalcogen substitution at the end groups of EDOT oligomers and demonstrated their impact on the crystal and electronic structures, as well as the enhanced conducting properties of the doped chalcogen-substituted oligomers. The introduction of end groups containing heavier atoms (such as Se and Te atoms) in the final step of the synthetic procedure may diversify the structures of these end groups, enabling the construction of rich and systematic oligomer libraries. The doped Se-substituted oligomers, denoted as **2O**-2SeMe•*X* (*X* = BF_4 and ClO_4), extended the conjugate area of the donor molecules, enhanced the intracolumnar transfer integral and ***W***, and reduced $\boldsymbol{U_{eff}}$. The ρ_{rt} of the **2O**-2SeMe•*X* compounds decreased by an order of magnitude in relation to that of S-substituted **2O**•*X,* owing to the reduction in the electronic correlation parameter, $\boldsymbol{U_{eff}/W}$, resulting from the extension of the conjugate system. The multiorbital system within the band structure, arising from the inversion of HOMO and HOMO–1 bands, may also significantly influence the electronic structures and physical properties of doped chalcogen-substituted oligomers. This study provides valuable insights into the design of oligomer-based conductors, with a particular focus on end groups, which can lead to the creation of a diverse array of structures that enhance conductivity. By strategically designing end groups to leverage high degrees of freedom of oligomer motifs, it is possible to expand the repertoire of oligomer-based conductor structures and achieve precise control over their conductive properties toward the development of diverse electronic devices with tailored functionalities.

Author Contributions

T.F. and H.M. directed this study. K.O., E.K. and S.Y. performed the synthesis procedures. K.O. performed electrical conductivity. K.O., T.M., T.Y., and H.Ok. performed the optical measurement. K.O. performed magnetic measurement. H.A., and O.Y. performed DSC. K.O., and H.Oi. performed the theoretical calculations for the band structures. K.O. performed single-crystal XRD analyses. K.O., T.F., and, H.M. wrote the manuscript, and all authors discussed the results and commented on the manuscript.

Conflicts of interest

There are no conflicts to declare.

Data availability

The crystallographic data (CIF files) for the structures reported in this article have been deposited with the Cambridge Crystallographic Data Centre (CCDC), under deposition numbers 2349871 (**2O**-2SeMe), 2349872 (**2O**-2SeMe•BF_4 at 293 K), 2352190 (**2O**-2SeMe•BF_4 at 123 K), 2349870 (**2O**-2SeMe•ClO_4 at 293 K), and 2352192 (**2O**-2SeMe•ClO_4 at 133 K). These data can be obtained free of charge via www.ccdc.cam.ac.uk/data_request/cif, or by emailing data_request@ccdc.cam.ac.uk, or by contacting The Cambridge Crystallographic Data Centre, 12 Union Road, Cambridge CB2 1EZ, UK; fax: +44 1223 336033. All experimental data within the article and its Supplementary Information are available from the corresponding authors upon requested.

Acknowledgments

This work was partially supported by JSPS Grants-in-Aid for Scientific Research (nos. JP16H04010, JP17K18746, JP18H05225, JP21K18597, and JP22H00106 to H.M.; JP20H05206, JP21K05018, and JP22H04523 to T.F.), Research Fellowships for Young Scientists (JP23KJ0577 to K.O.), JST PRESTO (JPMJPR22Q8 to T.F.), MEXT Grants-in-Aid for Scientific Research on Innovative Areas "Hydrogenomics" (JP18H05516 to H.M.), a research grant from Technology Foundation, the Naito Foundation, the Kao Foundation for Arts and Science to T.F., Fujimori Science and Technology Foundation to K.O., Amano Institute of Technology to K.O., and the University Fellowship Founding Project for Innovation Creation in Science and Technology from The University of Tokyo to K.O. The authors thank the Supercomputer Center, The Institute for Solid State Physics, and The University of Tokyo for use of the facilities. We thank Idemitsu Kosan Co., Ltd. for their support throughout the study.

References

1 A. Facchetti, *Chem. Mater.*, 2011, **23**, 733–758. DOI: 10.1021/cm102419z.
2 A. Elschner, S. Kirchmeyer, W. Lovenich, U. Merker and K. Reuter, *PEDOT | Principles and Applications of an Intrinsically Conductive Pol*, CRC Press, 2010.
3 S. Kirchmeyer and K. Reuter, *J. Mater. Chem.*, 2005, **15**, 2077. DOI: 10.1039/b417803n.
4 J. Ouyang, Q. Xu, C.-W. Chu, Y. Yang, G. Li and J. Shinar, *Polymer*, 2004, **45**, 8443–8450. 10.1016/j.polymer.2004.10.001.
5 A. M. Nardes, R. A. J. Janssen and M. Kemerink, *Adv. Funct. Mater.*, 2008, **18**, 865–871. DOI: 10.1002/adfm.200700796.
6 D. D. Graf, R. G. Duan, J. P. Campbell, L. L. Miller and K. R. Mann, *J. Am. Chem. Soc.*, 1997, **119**, 5888–5899. DOI: 10.1021/ja964345m.
7 T. Nishinaga and Y. Sotome, *J. Org. Chem.*, 2017, **82**, 7245–7253. DOI: 10.1021/acs.joc.7b00816, PubMed: 28650158.

 This journal is © The Royal Society of Chemistry 20xx

Please do not adjust margins

8 A. D. Jenkins, P. Kratochvíl, R. F. T. Stepto and U. W. Suter, *Pure Appl. Chem.*, 1996, **68**, 2287–2311. DOI: 10.1351/pac199668122287.
9 R. Kameyama, T. Fujino, S. Dekura, M. Kawamura, T. Ozaki and H. Mori, *Chem. Eur. J.*, 2021, **27**, 6696–6700. DOI: 10.1002/chem.202005333, PubMed: 33427364.
10 R. Kameyama, T. Fujino, S. Dekura and H. Mori, *Phys. Chem. Chem. Phys.*, 2022, **24**, 9130–9134. DOI: 10.1039/d2cp00250g, PubMed: 35388378.
11 R. Kameyama, T. Fujino, S. Dekura, S. Imajo, T. Miyamoto, H. Okamoto and H. Mori, *J. Mater. Chem. C*, 2022, **10**, 7543–7551. DOI: 10.1039/D2TC01216B.
12 K. Onozuka, T. Fujino, R. Kameyama, S. Dekura, K. Yoshimi, T. Nakamura, T. Miyamoto, T. Yamakawa, H. Okamoto, H. Sato, T. Ozaki and H. Mori, *J. Am. Chem. Soc.*, 2023, **145**, 15152–15161. DOI: 10.1021/jacs.3c01522, PubMed: 37395785.
13 T. Fujino, R. Kameyama, K. Onozuka, K. Matsuo, S. Dekura, K. Yoshimi and H. Mori, *Faraday Discuss.*, 2024, **250**, 348–360. DOI: 10.1039/d3fd00134b, PubMed: 37961785.
14 S. Kagoshima, H. Nagasawa and T. Sambongi, *One-Dimensional Conductors*, Springer-Verlag, BerlinHeidelberg, 1988. DOI: 10.1063/1.2811057.
15 J. Hubbard, *Proc. R. Soc. Lond. Ser. A: Math. Phys. Sci.*, 1997, **277**, 237–259.
16 K. Ido, K. Yoshimi, T. Misawa and M. Imada, *npj Quantum Mater.*, 2022, **7**, 1–10.
17 T. Tahara, S. Suzuki, M. Kozaki, T. Nishinaga and K. Okada, *Bull. Chem. Soc. Jpn.*, 2018, **91**, 1193–1195. DOI: 10.1246/bcsj.20180078.
18 C. D. Spicer, M. A. Booth, D. Mawad, A. Armgarth, C. B. Nielsen and M. M. Stevens, *Chem*, 2017, **2**, 125–138. DOI: 10.1016/j.chempr.2016.12.003, PubMed: 28149959.
19 M. J. Frisch, G. W. Trucks, H. B. Schlegel, G. E. Scuseria, M. A. Robb, J. R. Cheeseman, G. Scalmani, V. Barone, G. A. Petersson, H. Nakatsuji, X. Li, M. Caricato, A. V. Marenich, J. Bloino, B. G. Janesko, R. Gomperts, B. Mennucci, H. P. Hratchian, J. V. Ortiz, A. F. Izmaylov, J. L. Sonnenberg, D. Williams-Young, F. Ding, F. Lipparini, F. Egidi, J. Goings, B. Peng, A. Petrone, T. Henderson, D. Ranasinghe, V. G. Zakrzewski, J. Gao, N. Rega, G. Zheng, W. Liang, M. Hada, M. Ehara, K. Toyota, R. Fukuda, J. Hasegawa, M. Ishida, T. Nakajima, Y. Honda, O. Kitao, H. Nakai, T. Vreven, K. Throssell, J. A. Montgomery, Jr., J. E. Peralta, F. Ogliaro, M. J. Bearpark, J. J. Heyd, E. N. Brothers, K. N. Kudin, V. N. Staroverov, T. A. Keith, R. Kobayashi, J. Normand, K. Raghavachari, A. P. Rendell, J. C. Burant, S. S. Iyengar, J. Tomasi, M. Cossi, J. M. Millam, M. Klene, C. Adamo, R. Cammi, J. W. Ochterski, R. J. Martin, K. Morokuma, O. Farkas, J. B. Foresman and D. J. Fox, Gaussian 16, Revision B.01 Gaussian, Inc., Wallingford CT 2016.
20 T. Fujino, R. Kameyama, K. Onozuka, K. Matsuo, S. Dekura, T. Miyamoto, Z. Guo, H. Okamoto, T. Nakamura, K. Yoshimi, S. Kitou, T. Arima, H. Sato, K. Yamamoto, A. Takahashi, H. Sawa, Y. Nakamura, H. Mori, *Nature Comm.* in press. DOI: 10.1038/s41467-024-47298-1, PubMed: 38627402.
21 C. F. Macrae, I. Sovago, S. J. Cottrell, P. T. A. Galek, P. McCabe, E. Pidcock, M. Platings, G. P. Shields, J. S. Stevens, M. Towler and P. A. Wood, *J. Appl. Cryst.*, 2020, **53**, 226–235.DOI: 10.1021/j100785a001.
22 A. Bondi, *J. Phys. Chem.*, 1964, **68**, 441–451. DOI: 10.1002/jcc.1056.
23 G. te Velde, F. M. Bickelhaupt, E. J. Baerends, C. Fonseca Guerra, S. J. A. van Gisbergen, J. G. Snijders and T. Ziegler, *J. Comput. Chem.*, 2001, **22**, 931–967. DOI: 10.1002/jcc.1056.
24 OpenMX, http://www.openmx-square.org/.
25 R. Takagi, T. Hamai, H. Gangi, K. Miyagawa, B. Zhou, A. Kobayashi and K. Kanoda, *Phys. Rev. B*, 2017, **95**, 094420. DOI: 10.1103/PhysRevB.97.035101.
26 B. Brière, J. Caillaux, Y. Le Gal, D. Lorcy, S. Lupi, A. Perucchi, M. Zaghrioui, J.-C. Soret, R. Sopracase and V. T. Phuoc, *Phys. Rev. B*, 2018, **97**, 035101.
27 R. Takagi, H. Gangi, K. Miyagawa, E. Nishibori, H. Kasai, H. Seo, B. Zhou, A. Kobayashi and K. Kanoda, *Phys. Rev. Res.*, 2020, **2**, 033321. DOI: 10.1246/bcsj.20210230.
28 A. Kobayashi, B. Zhou, R. Takagi, K. Miyagawa, S. Ishibashi, A. Kobayashi, T. Kawamura, E. Nishibori and K. Kanoda, *Bull. Chem. Soc. Jpn.*, 2021, **94**, 2540. DOI: 10.1246/bcsj.20210230.
29 G. M. Sheldrick, *Acta Crystallogr. A Found. Adv.*, 2015, **71**, 3–8.
30 O. V. Dolomanov, L. J. Bourhis, R. J. Gildea, J. A. K. Howard and H. Puschmann, *J. Appl. Cryst.*, 2009, **42**, 339–341. DOI: 10.1107/S0021889808042726.
31 A. D. Becke, *Phys. Rev. A*, 1988, **38**, 3098–3100. DOI: 10.1103/PhysRevA.38.3098.
32 A. D. Becke, *J. Chem. Phys.*, 1993, **98**, 5648–5652. DOI: 10.1063/1.464913.
33 C. Lee, W. Yang and R. G. Parr, *Phys. Rev. B*, 1988, **37**, 785–789. DOI: 10.1103/PhysRevB.37.785.
34 R. Ditchfield, W. J. Hehre and J. A. Pople, *J. Chem. Phys.*, 1971, **54**, 724–728.
35 P. C. Hariharan and J. A. Pople, *Mol. Phys.*, 1974, **27**, 209–214. DOI: 10.1080/00268977400100171.
36 P. Fuentealba, H. Preuss, H. Stoll and L. Von Szentpály, *Chem. Phys. Lett.*, 1982, **89**, 418–422.
37 GaussView, Version 6.1, Roy Dennington, Todd A. Keith, and John M. Millam, Semichem Inc., Shawnee Mission, KS, 2016.
38 T. Ozaki, *Phys. Rev. B*, 2003, **67**, 155108. DOI: 10.1103/PhysRevB.67.155108.
39 T. Ozaki and H. Kino, *Phys. Rev. B*, 2004, **69**, 195113. DOI: 10.1103/PhysRevB.69.195113.
40 K. Lejaeghere, G. Bihlmayer, T. Björkman, P. Blaha, S. Blügel, V. Blum, D. Caliste, I. E. Castelli, S. J. Clark, A. Dal Corso, S. de Gironcoli, T. Deutsch, J. K. Dewhurst, I. Di Marco, C. Draxl, M. Dułak, O. Eriksson, J. A. Flores-Livas, K. F. Garrity, L. Genovese, P. Giannozzi, M. Giantomassi, S. Goedecker, X. Gonze, O. Grånäs, E. K. U. Gross, A. Gulans, F. Gygi, D. R. Hamann, P. J. Hasnip, N. A. W. Holzwarth, D. Iuşan, D. B. Jochym, F. Jollet, D. Jones, G. Kresse, K. Koepernik, E. Küçükbenli, Y. O. Kvashnin, I. L. M. Locht, S. Lubeck, M. Marsman, N. Marzari, U. Nitzsche, L. Nordström, T. Ozaki, L. Paulatto, C. J. Pickard, W. Poelmans, M. I. J. Probert, K. Refson, M. Richter, G.-M. Rignanese, S. Saha, M. Scheffler, M. Schlipf, K. Schwarz, S. Sharma, F. Tavazza, P. Thunström, A. Tkatchenko, M. Torrent, D. Vanderbilt, M. J. van Setten, V. Van Speybroeck, J. M. Wills, J. R. Yates, G.-X. Zhang and S. Cottenier, *Science*, 2016, **351**, aad3000. DOI: 10.1126/science.aad3000, PubMed: 27013736.
41 J. P. Perdew, K. Burke and M. Ernzerhof, *Phys. Rev. Lett.*, 1996, **77**, 3865–3868. DOI: 10.1103/PhysRevLett.77.3865, PubMed: 10062328.
42 K. Momma and F. Izumi, *J. Appl. Cryst.*, 2008, **41**, 653–658. DOI: 10.1107/S0021889808012016.
43 J. P. Perdew and Y. Wang, *Phys. Rev. B*, 1992, **45**, 13244–13249. DOI: 10.1107/S1600576719014092, PubMed: 32047413.
44 J. G. Snijders, P. Vernooijs and E. J. Baerends, *At. Data Nucl. Data Tables*, 1981, **26**, 483–509. DOI: 10.1103/PhysRevB.45.13244.

Data availability

The crystallographic data (CIF files) for the structures reported in this article have been deposited with the Cambridge Crystallographic Data Centre (CCDC), under deposition numbers 2349871 (**2O**-2SeMe), 2349872 (**2O**-2SeMe•BF_4 at 293 K), 2352190 (**2O**-2SeMe•BF_4 at 123 K), 2349870 (**2O**-2SeMe•ClO_4 at 293 K), and 2352192 (**2O**-2SeMe•ClO_4 at 133 K). These data can be obtained free of charge via www.ccdc.cam.ac.uk/data_request/cif, or by emailing data_request@ccdc.cam.ac.uk, or by contacting The Cambridge Crystallographic Data Centre, 12 Union Road, Cambridge CB2 1EZ, UK; fax: +44 1223 336033. All experimental data within the article and its Supplementary Information are available from the corresponding authors upon requested.